Master of Science Thesis

Activity quantification of planar gamma camera images

Marie Sydoff

Supervisor: Sigrid Leide-Svegborn

The work has been performed at
Department of Radiation Physics
Malmö University Hospital

Medical Radiation Physics
Clinical Sciences, Lund
Lund University, 2006

Contents

Abstract

Determination of absolute activity of ^{99m}Tc and ^{123}I in organs for the purpose of patient-specific dosimetry in nuclear medicine examinations and therapy is of great importance. In order to make accurate quantification of the organ content from planar gamma camera images of phantoms, several corrections has to be made.

The accuracy of a number of correction methods and different combinations of these were evaluated in phantom studies of liver, kidneys and heart. Correction was made for attenuation by transmission measurements. Three different scatter correction methods were used; the Triple Energy Window method (TEW), the Double Energy Window method (DEW) and the Lower Energy Window method (LEW). For background correction three different methods were used; 1. Gates correction method (conventional correction method); 2. Kojima method (with organ thickness and depth at which the organ is placed taken into account); and 3. Bujis correction method (organ thickness and body thickness taken into account). Attenuation correction was made for all measurements, and each of the three scatter corrections were combined with each of the three background corrections to find the most suitable set of correction methods.

The accuracy of the estimations of organ activity is highly dependent of the correction methods used. Applying background correction in conjunction with scatter correction gave an underestimation ranging between 22% and 0.3% (for ^{99m}Tc and all organs) depending on the correction methods used. For ^{123}I, these values ranged between an overestimation of 12% and 1.4%. For higher background activities, the deviation from the true activity values became higher, but reasonably accurate. The most consequent results when considering all organs and organ-to-background activities was found when applying the LEW scatter correction method combined with the Bujis background correction method.

1 Introduction

Determination of absolute activity in organs for the purpose of patient-specific dosimetry in nuclear medicine examinations and therapy is of great importance. In order to make an accurate quantification of the organ activity content from scintillation camera images, several corrections has to be made. The purpose of this work was to investigate these correction methods on the basis of planar gamma camera images of the heart, liver and kidneys. It is important that this technique for activity quantification is optimized in order to get more accurate internal dose estimates for radionuclide therapy and -examinations. New radiopharmaceuticals also have to be controlled with respect to risks and therapeutic effects. The reason for using planar gamma camera images and not tomographic SPECT images is that this technique is simpler and less time demanding, which is an important advantage in health service.

In order to optimize the technique for quantification i.e, to achieve the most suitable set of correction methods, several methods were tested in phantom studies. In the first step, corrections for attenuation of gamma radiation in the phantom was made with a transmission based attenuation correction method. This method includes measurements performed on a ^{57}Co flood source with and without phantom to obtain values of the attenuation in the phantom. The conjugate view approach were used, i.e the counts combined from one anterior and one posterior image was used to make the quantification. For calculation of the activity, the so-called Fleming's formula were used [1].

In step two, both attenuation- and scatter correction were made. Scatter correction is important, since it reduces the influence of patient size and thus reduces the deviation from the true activity value [2]. For scatter correction three different methods were used. These were a Dual-energy-window (DEW) method, a Triple-energy-window (TEW) method and a third method that were a combination of these two methods called the LEW-method. This method has been proposed by Ljungberg *et al.* [4] to be a method that gives a more accurate result than the formerly used TEW method. The TEW method is a regularly used scatter correction method, and is in this study compared with the two methods mentioned above to determine which one of these, together with the appropriate background correction method is the most suitable for this kind of measurements.

In the third set of correction methods the activity values were corrected for attenuation and scatter plus for the influence of the activity in overlapping organs and in surrounding tissue, so-called background activity. The

conventional background subtraction is performed by subtracting the count rate in an adjacent region of interest, (ROI), from the count rate in the ROI which is placed over the organ in question. Two other background correction methods were also used; the Kojima and the Bujis method in order to get a comparison between these three different background correction methods. The Kojima method includes correction for organ thickness and takes the depth at which the organ is placed into account. In the Bujis method, the thickness of the organ and also the total body thickness is taken into account. For all different methods, organ-to-background concentration ratios of infinity, 10:1, 5:1 and 2:1 were achieved.

2 Background

In the nuclear medicine area several studies have been performed in order to optimize the methods of absolute activity quantification, [2, 4, 5, 7]. These studies have shown reasonable results for some of the methods used in this study but the set of correction methods which gives the most optimal correction is yet to be found.

There are a number of sources of errors that makes the activity quantification complicated. Determination of the activity in an organ can be obtained by using the so-called conjugate view method. In this method one anterior and one posterior image is acquired and a region of interest, (ROI), is drawn over the organ of interest in each image. The geometric mean of the count rates in these ROI: s are then calculated to determine the activity content of the organ in question. But this method leaves a few questions. For example: which amount of the gamma radiation is attenuated within the surrounding tissue? Should the organ thickness be considered, and is this valid for all organs? How much does the sensitivity of the camera system influence the quantification? What influence does background activity have on the accuracy of the calculations?

According to Fleming [1] the activity A in an organ or tissue is given by the expression

$$A = (N_a \cdot N_p)^{1/2} \left[\left(e^{-\mu_e \cdot \frac{L}{2}} \cdot \frac{\sinh(\mu_e \cdot \frac{l}{2})}{\mu_e \cdot \frac{l}{2}} \right) K \right]^{-1} \tag{1}$$

Where N_a and N_p are the count rates in the anterior and posterior images respectively, L is the body thickness and l is the organ thickness. μ_e is the lin-

ear attenuation coefficient and K is the sensitivity of the camera/collimator system.

As mentioned earlier, to find out the count rate of the anterior and posterior image is necessary. To make an expression giving the count rate detected by the gamma camera in one of the images one can assume a bar of uniformly distributed activity in the body. If this bar is imaged perpendicular to the camera surface, the count rate for the anterior image is given by the expression

$$N_a = K \cdot A \cdot e^{-\mu_1 \cdot a} \int_0^l e^{-\mu_2 \cdot x} \cdot dx \tag{2}$$

In this expression the detector sensitivity K and also the attenuation in the tissue and organ is taken into account [1]. The term $e^{-\mu_1 \cdot a}$ accounts for attenuation in the surrounding tissue, the integration term $\int_0^1 e^{-\mu_2 \cdot x}$ is the attenuation in the bar of uniformly distributed activity and a is the distance between the anterior surface of the body and the anterior surfase of the bar. The latter estimates how much the radiation attenuates in the organ of interest. After integration of the last term in expression 2 the count rate is given by

$$N_a = \frac{K \cdot A \cdot e^{-\mu_1 \cdot a}}{\mu_2} \left[1 - e^{-\mu_2 \cdot l}\right] \tag{3}$$

In this equation μ_1 is the linear attenuation coefficient of the bar and μ_2 is the attenuation coefficient of the surrounding tissue. A similar expression is obtained in the same way for the posterior count rate, and the geometric mean of these count rates is acquired by the following calculations

$$\left.\begin{array}{l} N_a = \frac{K \cdot A \cdot e^{-\mu_1 \cdot a}}{\mu_2} \left[1 - e^{-\mu_2 \cdot l}\right] \\ N_p = \frac{K \cdot A \cdot e^{-\mu_1 \cdot b}}{\mu_2} \left[1 - e^{-\mu_2 \cdot l}\right] \end{array}\right\}$$

$$(N_a \cdot N_p)^{1/2} \Longrightarrow \frac{K \cdot A \cdot e^{-\mu_1 \frac{(a+b)}{2}}}{\mu_2} \cdot \left(1 - e^{-\mu_2 \cdot l}\right) \tag{4}$$

The use of the following expression

$$\sinh x = \frac{e^x - e^{-x}}{2} \tag{5}$$

and an approximation that the linear attenuation coefficient in the bar and the surrounding tissue are considered equal admits that equation 4 can be rewritten as

$$(N_a \cdot N_p)^{1/2} = K \cdot A \frac{\sinh(\mu_e \cdot \frac{l}{2})}{\mu_e \cdot \frac{l}{2}} e^{-\mu_e \frac{L}{2}} \tag{6}$$

Where the term

$$\frac{\sinh(\mu_e \cdot \frac{l}{2})}{\mu_e \cdot \frac{l}{2}}$$

is the source organ thickness correction term, which is employed to correct for self-attenuation in the organ. Na and Np is the number of counts in the anterior and posterior image respectively. L corresponds to body thickness at the region of interest, and l is the organ thickness, both measured in cm. K is the sensitivity of the gamma camera system, i.e the count rate per unit activity, measured in cps/MBq [1]. Expression 6 can then be solved for the activity A to obtain the above equation 1, which is used for calculation of the activity in the organ of interest. If this relation is used as here, and no other correction is made, it gives an overestimation of the activity. The use of this expression gives an overestimation, which is clear when considering that the term

$$\frac{\sinh(\mu_e \cdot \frac{l}{2})}{\mu_e \cdot \frac{l}{2}} \geq 1$$

The overestimation will also be larger as the organ of interest, i.e. the source organ itself, gets thicker. This is why the use of several correction methods is needed. Corrections must be made for attenuation, scatter in the phantom and in the gamma camera couch, background correction and also correction for activity in overlapping structures. The different correction methods are explained in the sections 3.5 - 3.7 below.

2.1 The gamma camera

In nuclear medicine imaging the goal is to produce an image of the distribution of the administered radiopharmaceutical in the body of a patient. This is carried out with a gamma camera often equipped with a parallel hole collimator.

The radiopharmaceutical is administered to the patient usually by an intravenous injection, but in some cases orally or by inhalation. The gamma radiation which emanates from the radioactive decay of the radiopharmaceutical in the body strikes the collimator on its way towards the scintillation crystal and PM tubes in the detector.

In order to only measure the photons perpendicular to the NaI(Tl)-crystal, the detector is equipped with a collimator which consists of a large lead sheet perforated with thousands of holes, or channels, with a specific length and width. If the photon energy is suitable for the collimator chosen, only the photons that are almost perpendicular to the surface is let through the holes.

When the photons have traveled through the holes of the collimator, they strike the scintillation crystal and are converted into visible light photons, which are detected by a collection of photomultiplier tubes, (PMTs), placed behind the scintillation crystal. The PMTs are used, as the name implies, for multiplying the electrons that are produced by the scintillation light into a measurable electrical current which is defined as a *count*.

From the PM tubes the signals that have a magnitude within a predetermined range are sent on for further processing in the computer to form an image.

2.2 Detector sensitivity

The PM tubes can sometimes have variation in sensitivity and this can introduce a source of error, which will affect the activity quantification negatively. The sensitivity of the gamma camera has to be determined so that this can be avoided. An image is obtained of a known amount of activity in for example a petri dish. One measurement can be done with each gamma camera and the sensitivity is calculated as counts per second /MBq of true activity in the dish.

When measuring the activity in the syringe before a measurement an activity meter or a lead-shielded Ge - detector can be used.

2.3 Transmission based attenuation correction

Transmission measurements are done to determine the attenuation in the phantom or patient . For this, a ^{57}Co flood source can be used. The detectors of the dual-headed gamma camera is placed in a 180 ° geometry. The flat source is placed directly onto the lower detector surface, so that the gamma radiation can go through both the phantom and the gamma camera coach on its way to the upper detector. Only the upper detector is used in these transmission measurements. To determine the attenuation in the material, two transmission images must be obtained. One measurement including the phantom/patient but without activity is obtained to determine the attenuated count rate N. The second measurement is done without phantom/patient on the couch to determine the original count rate N_0.

The attenuation of the count rate N is defined as

$$N = N_0 \cdot B(x) \cdot e^{-\mu x} \tag{7}$$

where μ is the attenuation coefficient of the material in question and x the thickness of the material [6]. B(x) is the build-up factor, by which the influence of scattered photons is considered.

The Build-up factor can, however, be replaced by a lower value of μ, which is called μ_{eff}; the effective attenuation coefficient.

$$N = N_0 \cdot e^{-\mu_{eff} x} \tag{8}$$

The fraction of the attenuated and the original count rate gives the attenuation and the effective attenuation coefficient can easily be calculated with the presence of these values

$$\frac{N}{N_0} = e^{-\mu_{eff} x} \Longrightarrow \mu_{eff} = \frac{-ln(N/N_0)}{x} \tag{9}$$

If the emission measurements are done with another radionuclide (Y), than the transmission measurements (radionuclide X), a transformation must be made in order to achieve the proper attenuation coefficients regarding the radionuclide in question. If one consider the amount of scatter to be the same from radionuclide X and Y, the transformation is given by

$$\mu_{eff_Y} = \frac{(\frac{\mu}{\rho})_Y \cdot \mu_{eff_X}}{(\frac{\mu}{\rho})_X} \tag{10}$$

2.4 Scatter correction

When gamma-ray photons of lower energies travels through a patient or a phantom from a source organ, they interact with the soft tissue mainly by Compton scattering. Every time the photon is scattered an amount of energy is lost to an electron and the loss of energy increases as the scattering angle θ increases, as shown by the expression for the energy of the scattered photon $h\nu'$

$$h\nu' = \frac{h\nu}{1 + \frac{h\nu}{mc^2}(1 - cos\theta)} \tag{11}$$

Where θ is the scattering angle, m is the electron mass and c is the speed of light in vacuum. The photons can also be scattered several times, [8].

When using a gamma camera an energy window is centered around the photopeak in order to allow only the photons with an energy within this interval to be detected as a true event. All the events detected within this interval are not primary photons. A certain amount of these photons are scattered photons and some can have been scattered several times before reaching the detector. This gives rise to a blur in the image, i.e. lower image contrast. It is therefore important that the amount of scatter is known in order to make an accurate activity quantification. In this study three different types of so-called energy domain window methods are used to correct for scatter. When using this type of methods, with subwindows adjacent to the photopeak, scattered photons originating from sources not within the FOV can be considered.

2.4.1 Dual-energy window method

One way of determining the scattered events detected within the energy boundaries that limits the photopeak window, is by using the DEW method. This method has been used in other studies, and was shown a reasonable result of scatter correction even though the TEW method, (which is discussed in the next section), is shown to be a more accurate method [9, 4]. Despite

this, the accuracy of this method has to be studied and compared again in order to get a better statistical significance of the results.

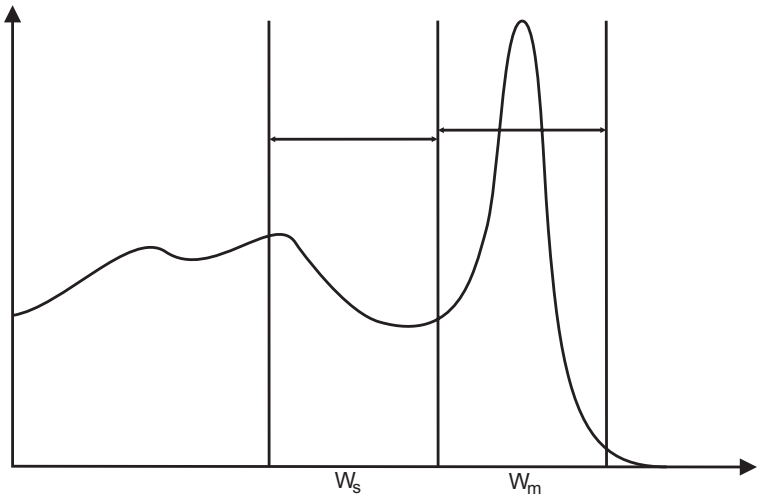

Figure 1: Energy window settings for the Dual-energy window method with a main window of 20 % and a lower scatter window of 28 keV.

When using the DEW method, a main window can be set to 20% around the photopeak, and a lower scatter window of 28 keV is placed left of and adjacent to the main window. The number of scattered events in the main window is determined assuming that the number of scattered photons in the main window is proportional to the number of scattered photons in the lower scatter window and is thus given by

$$S_m = k \cdot S_{low} \tag{12}$$

where S_m is the scattered photons in the main window, S_{low} the scattered photons in the lower window and k is a proportional constant that gives the quantitative difference between the scattered events in the two windows respectively, (k = 0.5 as suggested by Jaszczak *et al.* [**?**] and also used by Ljungberg *et al.* [4]). k depends on the width of the scatter window, the placement of the source and the energy resolution of the gamma camera.

When images has been acquired and the total number of counts in an organ ROI for the main window image is determined, the value of S_{main} is subtracted from the total number of counts in order to get the number of primary events in the ROI.

2.4.2 Triple-energy window method

The TEW method is a method that was shown by Ogawa *et al.* [2] to be more accurate than the above mentioned DEW method. The difference in this method, from the DEW method, is the use of two energy windows adjacent to the photopeak window, instead of only one, (see figure. 2). The main energy window is set to 20% around the photopeak and two narrow energy windows are placed adjacent to the main window on the upper and the lower side respectively. The number of scattered counts to be subtracted from the number of counts in the main window is then given by

$$S_m = \left(\frac{S_{low}}{W_s} + \frac{S_{up}}{W_s} \right) \frac{W_m}{2} \tag{13}$$

where S_{low} and S_{up} is the number of events detected in the lower and upper energy window respectively and W_s is the width of the scatter windows. Further on, W_m is the width of the main window and S_{main} is the number of scattered events in the main window [9, 2].

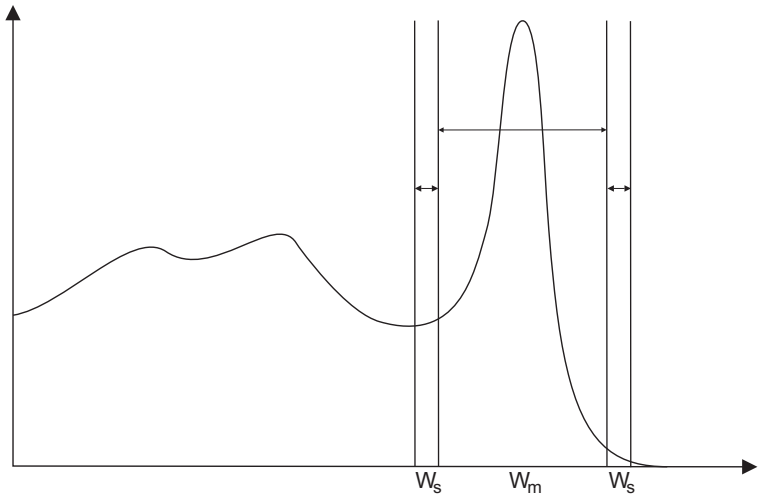

Figure 2: Energy window settings for the Triple-energy window method with a main window of 20 % and two narrow scatter windows adjacent to the main window.

2.4.3 Lower-energy window method

The use of an energy window placed on the higher energy side of the main window can, however increase image noise. The proportion of primary pho-

tons to the total amount of photons in this window is large if compared to the lower energy window. If the counts in the higher energy window is subtracted from the counts in the main window, many counts from primary photons also is subtracted and thus results in a less accurate activity quantification. To avoid this problem, the higher window can be set to 0 as suggested by Ljungberg *et al.* [4]. This gives that the method includes a main window of 20% around the photopeak, and a lower, narrow energy window adjacent to the main window.

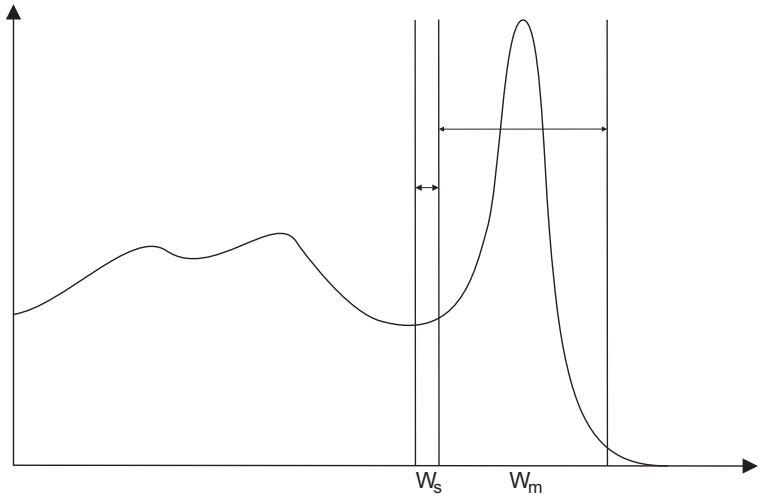

Figure 3: Energy window settings for the Lower-energy window method with a main window of 20 % and a lower scatter window of 7 keV.

The amount of scattered photons detected within the main energy window, is calculated as above, (equation 13), with the exception of the second term in the parenthesis. S_{main} is then given by

$$S_m = \frac{S_{low}}{W_s} \cdot \frac{W_m}{2} \tag{14}$$

The amount of scattered photons, which are calculated above, are then subtracted from the total number of counts detected in the main window.

2.5 Background correction

One complication in nuclear medicine imaging is that the activity is not only distributed to the organs of interest, but also to over- and underlying tissue and circulating blood. This may cause an overestimation of activity in the

organ ROI if not corrected for. The three most commonly used correction methods, which also are used in this study, is explained below. The reason that these methods are commonly used is that they are easy to implement and gives reasonable results.

2.5.1 Gates method

Conventional background correction, referred to as the Gates' method, is the simplest method of subtracting the count rate due to background activity. The background activity is assumed to be homogeneous and an ROI is drawn adjacent to the organ of interest to determine the count rate in this region. In this method the background activity is determined as the number of counts per pixel in this ROI multiplied with the background count rate [10]. The background count rate is then subtracted from the count rate in the organ of interest in the anterior image as follows

$$N_a^* = N_a - N_{bgr} \tag{15}$$

where N_a is the count rate in the organ of interest in the anterior image, N_{bgr} is the background count rate and N_a^* is the background corrected count rate in the anterior image. This is equivalent for the count rate in the posterior image. This method is simple to perform, but it makes an overcorrection and therefore gives an underestimation of the actual activity in the organ of interest since it does not take the thickness of the organ into account.

2.5.2 Kojima method

Another method of background correction is the Kojima method [11]. This method takes into account the size of the organ of interest and the depth at which the organ is located. It also assumes that the background activity concentration is homogeneous.

To determine the thickness of an organ in a patient, a lateral image can be obtained and the thickness measured in the lateral image. If the organ phantom is irregular in shape towards the detector surface, which means that the source - detector distance is inconsistent, a so called *effective thickness* can be calculated. The effective thickness, (l_{eff}), can be defined as one side of a rectangle when the other side is equal to the diameter of the circular cross section,(D), of the phantom and also has the same area as this cross section, (πr^2). This gives that

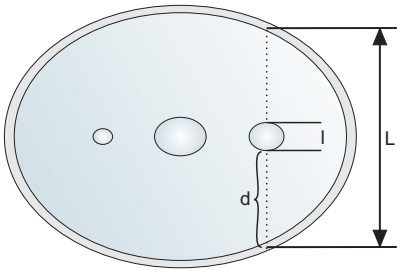

Figure 4: Background activity correction using the Kojima method. L is the body thickness, l the organ thickness and d is the distance between the posterior surface of the body and the posterior surface of the organ, all measured at the source ROI.

$$l_{eff} = \frac{\pi r^2}{D} \tag{16}$$

and this is used in the correction terms for the count rate in the anterior and posterior images as follows below. The effective thickness can be calculated for the big cylinder phantom, (the body thickness L), or it can be measured at the source ROI [5].

To correct for the underestimation of activity that follows from the Gates' method, the count rate in the source ROI has to be adjusted with the count rate in the background ROI as in the conventional background correction method, (equation 15), but with the difference that the background count rate, (N_{bgr}), is multiplied with a correction factor, ($C_{a,p}$), regarding the organ thickness for the anterior and posterior count rates respectively.

$$N_a^* = N_a - N_{bga} \cdot C_a$$

$$N_p^* = N_p - N_{bgp} \cdot C_p \tag{17}$$

were N_a^* and N_p^* are the count rates that are corrected for background activity, N_a and N_p are the measured count rates for the anterior and posterior image respectively and N_{bga} and N_{bgp} are the respective background count rates for the organ ROI:s. C_a and C_p in the above expressions are defined as follows

$$C_a = 1 - \frac{e^{-\mu_0(L-d-l_{eff})} \cdot (1 - e^{-\mu_0 l_{eff}})}{1 - e^{-\mu_0 L}}$$

$$C_p = 1 - \frac{e^{-\mu_0 d} \cdot (1 - e^{-\mu_0 l_{eff}})}{1 - e^{-\mu_0 L}} \tag{18}$$

In these expressions, d is the distance between the posterior surface of the body phantom at the source ROI and the posterior surface of the organ phantom and l_{eff} and L is the organ thickness, and body thickness at the source ROI respectively. μ_0 is the narrow beam linear attenuation coefficient.

2.5.3 Bujis method

The Bujis method is a simpler method of background correction than the Kojima method. Despite this, it has shown to give results that is more correct than the ones achieved after the use of Gates method and that are comparable with those obtained when using the Kojima method [5]. This method of correction also takes the thickness of the organ of interest, l, into account, and instead of the depth at which the organ is located, it makes corrections for the total body thickness, L. In a similar manner as the above explained Kojima method, the background count rates are multiplied with a correction factor to avoid an overestimation of the background activity that is a consequence of the fact that the organ thickness is not negligible. The correction of the measured count rates in the anterior and posterior images respectively is showed by the below expressions

$$N_a = N_a^* - N_{bga} \cdot F$$

$$N_p = N_p^* - N_{bgp} \cdot F \tag{19}$$

where N_a, N_p, N_a^*, N_p^*, and N_{bga} and N_{bgp} is the same as in equation 17. The correction factor F, applicable on both the anterior and posterior count rate, is defined as follows

$$F = 1 - \left(\frac{t_{eff}}{T_{eff}}\right) \tag{20}$$

where t_{eff} is the effective organ thickness in question and T_{eff} is the effective total body thickness [5, 7].

2.6 Overlapping organs

If an image contains organs that overlap each other, this must be corrected for to obtain the true activity in the organ of interest. When an ROI is drawn over the organ of interest, an over- or underlying structure also containing activity sometimes is included. The activity of this region must be separately calculated. If one of the kidneys and the liver is overlapping, the count rate in the other kidney can be determined and this can be applied to the first kidney, assuming the same activity concentration in both kidneys.

The number of counts in the overlapping part of the kidney can be calculated by the following procedure: Determine the number of counts per pixel in the ROI that is drawn over the non-overlapping part of the left kidney and multiply this with the number of pixels in the right kidney, which is not overlapping any part of the liver. Subtract the total number of counts in the left kidney ROI from the total number of counts in the right kidney ROI and then an approximation of the activity in the overlapping part of the organ is estimated. In this method a homogeneous activity distribution in the kidney is assumed [6, 7].

3 Material and methods

3.1 Detector sensitivity

Two different radionuclides were used in the measurements; ^{99m}Tc and ^{123}I. The characteristics of these radionuclides are presented in table 1.

Table 1: Characteristics for the radionuclides in this study.

Radionuclide	Halflife	Decay	Photon energy
^{99m}Tc	6.02 h	IT	140 keV
^{123}I	13.2 h	EC	159 keV

The planar sensitivity of the detector system defined as the observed count rate per unit activity (cps/MBq), was determined.

The measurements were carried out with a dual-headed gamma camera, (Variable angle emission imaging system, Siemens e-cam), with a Low Energy High Resolution, (LEHR), parallel-hole collimator. The energy window was

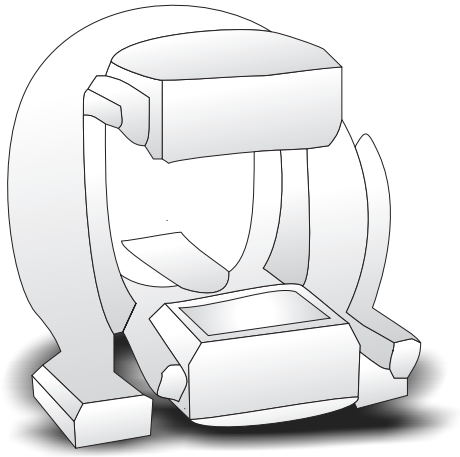

Figure 5: The dual-headed gamma camera in a 180 ° geometry, which is used for all measurements in this study.

15% centered around 140 keV for ^{99m}Tc and 159 keV for ^{123}I. A filter paper was soaked with thoroughly measured activity (ionization chamber, Capintec Inc. Ramsey, New Jersey) and placed in a petri dish. The petri dish was placed in the center of the Field-of-view (FOV) directly onto the detector. An acquisition was then performed for five minutes yielding one anterior and one posterior image. A ROI was drawn in the anterior image around the visible activity in the petri dish. The same ROI was then used in the posterior image. The total number of counts from the activity in the petri dish was noted as the number of counts/pixel multiplied with the number of pixels in the ROI. The number of counts in the background region was found by moving the ROI outside the visible activity and multiplying the number of pixels with the number of count/pixel in this region. Correction was also made for radioactive decay between the time of activity measurement and the time of acquisition (300s) with the gamma camera.

A second sensitivity measurement was carried out with the images acquired using a whole body scan procedure, with parameters same as used in the measurements on the thorax phantom. A sensitivity measurement was made with a whole body scan for both ^{99m}Tc and ^{123}I for use in the activity quantification of both radionuclides.

3.2 Phantom measurements

The phantom that were used in the first measurements was a large cylinder perspex phantom with a diameter of 21.5 cm and a height of 18 cm (Figure 6).

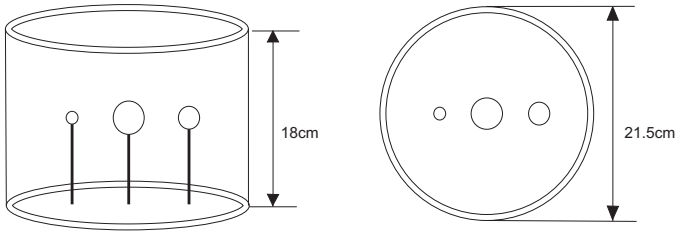

Figure 6: Dimensions of the cylindrical perspex phantom used in the first measurements.

Three spheres of different sizes were placed inside the phantom and attached by rods to the bottom of the cylinder. The volume of the spheres was 19.2 ml, 11.4 ml, and 5.7 ml respectively. The exact volume of the spheres was determined by weighing the spheres before and after filling them with thoroughly determined activity.

In the second part of the phantom measurements, a human-like phantom simulating the torso of a 70 kg man; a MIRD phantom, was used. The length of the torso phantom was 68 cm, width 40 cm, maximum thickness 20 cm and the volume was 40 liters. Into this torso phantom, lung-, heart-, kidney- and liver phantoms were placed (figure 7). A plastic tube filled with water, (and later with activity), was placed over part of the liver to simulate an overlapping structure. The size of the organ phantoms was determined so that the replacement volume of them could be established. This volume could then be subtracted from the total volume of the torso phantom in order to determine the amount of water surrounding the organs.

Activity was added to this surrounding water in various concentrations to make a simulation of background activity. The lung phantoms were filled with styrofoam beads in order to simulate the lower density of lung tissue and yielding an attenuation corresponding to the attenuation in normal lung tissue. The length of the lung phantom was 25 cm, the maximum width 15.5 cm and the volume was 2.26 l. The lung phantom also included a plug which volume was 140 ml. So the total replacement volume of one lung was 2.4 litres.

Two small cylinders simulating the kidneys were used. Each of the cylinders had a diameter of 6 cm and a length of 7.7 cm. The volume were 217 ml. The two cylinders were put together with a smaller cylinder with a volume of 17 ml, which gave a total volume of 234 ml.

The heart phantom had a volume of 329 ml. The replacement volume of the liver phantom was a total of 2400 ml.

Figure 7: The MIRD phantom. Placement of the organ phantoms inside the torso phantom during the measurements for both ^{99m}Tc and ^{123}I.

Figure 8: Left: liver phantom with small intestine phantom. Right: heart phantom.

3.3 Measurements on the cylinder phantom

In the first measurements a simple cylinder phantom was used. This was done in order to minimize the sources of error and to try out the best way to perform the measurements on the human-like phantom. The cylinder phantom, simulating the thorax of a 70 kg man was filled with water and sealed. The three spheres of various sizes, imitating malignancies, were filled with thoroughly determined activity an placed into the cylinder phantom.

Transmission measurements were performed with a ^{57}Co flood source placed directly onto the lower detector when the two detectors were placed in a 180 ° geometry as shown in figure 5.

First, a transmission image of the gamma camera coach was taken. The next image obtained was of the water filled, cylindrical phantom with no

activity (only water) in the spheres or in the background placed on the gamma camera couch. The last image taken was of the water filled phantom with activity in the spheres.

Around each sphere on the image an ROI was drawn and the number of counts and the number of pixels of each of these were noted. The same ROI:s were copied to the image taken of only the water filled phantom. In order to determine the attenuation in the phantom the counts per pixel in the water filled phantom without activity was determined for each of the sphere ROI:s, and these values were then used as N in equation 8. N_0 in the same expression were the count rate obtained from the ROI:s in the image without the phantom.

Since the gamma photons from ^{99m}Tc and ^{57}Co have different energies; 140 keV and 122 keV respectively, a transformation of the attenuation calculations was made of the values from the transmission measurement. This transformation is given by the above equation 10.

In the emission measurements, the images were taken as whole body scans, with a scan speed of 15 cm/min. and a scan length of 100 cm. The detectors were placed in a 180° geometry.

3.4 Measurements on the MIRD phantom

The organ phantoms were filled with ^{99m}Tc and ^{123}I respectively, with activity amounts similar to the activity uptake in the human body during an ordinary nuclear medicine examination and placed inside the torso phantom as shown in figure 7. The phantom was placed on the gamma camera couch in a 180° gamma camera geometry. The images were obtained using a whole body scan procedure, (scan speed 15 cm/min, scan length 100 cm).

Anterior and posterior images of the solely water filled torso phantom including the organ phantoms containing activity of various concentration were taken. The main energy window was set to 20 % centered about the photopeak, (140 keV for ^{99m}Tc and 159 keV for ^{123}I). Measurements were done with one main energy window and two narrow energy windows placed adjacent to the main window on the upper and the lower side of the main window respectively for use in the TEW scatter correction. One image of the detected counts in each energy window was obtained. One set of images was obtained using one main energy window and one lower scatter window placed left of and adjacent to the main window for use in the DEW scatter correction. The last measurement were carried out with the LEW method, which includes one main window and a lower, narrow energy window adjacent to the main window. All measurements were done with three different organ-

to-background activity concentration ratios.

3.4.1 Attenuation correction

To make an attenuation correction, a transmission measurement was done with a ^{57}Co flat source and a water filled phantom as described above in 3.3. In the images that was obtained in the transmission measurement, ROI:s corresponding to each organ was drawn in both images, (with and without phantom between the detector and the flood source). The count rate / pixel was determined for each organ and multiplied with the number of pixels in the corresponding ROI in the image without the phantom. The term $e^{-\mu_e(\frac{L}{2})}$ in equation 1, was used for calculation of the attenuation. The count rate in the image with and without the phantom was N_0 and N respectively, (L was the body thickness). The different photon energies of ^{57}Co and ^{99m}Tc and ^{123}I was taken into consideration, as described in 3.3.

3.4.2 Scatter correction

In this study, three scatter correction methods were implemented: The Triple energy window method (TEW), the Dual energy window method (DEW) and the Lower energy window method (LEW).

- For the TEW scatter correction three energy windows were used, (one main window of 20% and two narrow windows of 7 keV each). One image of the count rates in each energy window was obtained. In each of these images ROI:s were drawn around the liver, kidneys, heart and intestine. The count rate / pixel in the ROI:s in the scatter images were multiplied with the number of pixels in the ROI:s drawn in the main image. The scatter correction was carried out according to equation. 13. The scattered count rates that was calculated in this way was subtracted from the count rate in the main energy window.

- Two energy windows were used for the DEW scatter correction measurement. The main energy window of 20% around the photopeak and a scatter window (a lower energy window of 28 keV). To make the correction, the count rates were achieved in the same way as described for TEW (the count rate / pixel in the ROI:s in the scatter image were multiplied with the number of pixels in the ROI:s drawn in the main image). The count rates for every organ calculated from the scatter image was multiplied with a factor 0.5 [3] and subtracted from the count rate for each organ in the main image.

- The LEW method included two energy windows: a main window of 20% and a lower scatter window of 7 keV. The correction was made in the same way as for the TEW method above, with the exception of the upper energy window, which was not present in this measurement. The ratio of the count rate in the scatter window and the width of the scatter window was multiplied with half of the main energy window width. This gave the scattered count rates that was subtracted from the count rate in the main window. The count rate / pixel of the ROI:s in the scatter window were achieved by multiplying the count rate / pixel in the ROI:s in the scatter image with the number of pixels in the ROI:s drawn in the main image.

3.4.3 Background correction

Three different background correction methods were considered: the conventional background correction method, (Gates method) [10], the Kojima method [11], which accounts for the size of the organ and the depth at which the organ is located and the Bujis method [5], which accounts for organ size and the total body thickness. Every background correction were made in conjunction with each scatter correction to compare the accuracy of the results depending on which two methods are combined. Three different background activity concentration ratios were used.

- Correction of the background activity by the Gates method was carried out for small organs as the heart and kidneys by copying the ROI which was drawn over the organ of interest and placing it adjacent to the organ. The background ROI was also placed at the same position as the organ in the length direction in order to get the same body thickness at the placement of the organ ROI as for the background ROI. The count rate in the background ROI was subtracted from the count rate in the organ ROI.

  If the organ was larger, as for the liver, the background ROI had to be smaller than the organ ROI to avoid that activity from some of the other organs was included in the activity estimations of the background ROI. The count rate / pixel in the background ROI was multiplied with the number of pixels in the organ ROI and this background count rate was subtracted from the count rate in the organ ROI.

  A small intestine, also containing activity, was placed over a part of the liver to simulate an overlapping structure. ROI:s were drawn over the overlapping part and the non-overlapping part separately. In order to

calculate the count rate that had to be subtracted from the count rate in the liver ROI, the count rate / pixel in the non-overlapping part of the small intestine was determined and multiplied with the number of pixels in the overlapping part.

- To make the Kojima background correction, the count rates from the ROI:s described above were used. With this correction method, the organ size was taken into account and the background count rate was multiplied with the correction factor C_a for the anterior image and C_p for the posterior image, (defined in eq. 18). The corrected count rates were subtracted from the count rates in the organ ROI:s.

- Correction for organ size and body thickness was made with Bujis background correction method. The background ROI:s were drawn as above and the count rates were used to calculate the correction factor F, (eq. 20). The correction factor F was multiplied with the background ROI count rate and multiplied with the organ count rate for each organ.

4 Results

4.1 Detector sensitivity: static

The activity of ^{99m}Tc in the syringe was measured in a well-type ionization chamber, (Capintec inc. Ramsey, New Jersey), to 41.3 MBq. The activity was corrected for physical decay. The number of counts in the ROI around the activity was subtracted with the activity in the same ROI placed outside and adjacent to the activity to correct for background activity. The sensitivity of each detector were calculated as

$$\Rightarrow K \approx 86.6 \ cps/MBq$$

4.2 Detector sensitivity: scanning

Since the sensitivity depends on the system parameters, all parameters are the same as for the emission measurements. The detector geometry was 180°. A whole body scan was carried out with a scan speed of 15 cm/min and a scan length of 100 cm. The matrix size was 256 x 1024. The petri dish containing 67.4 MBq ^{99m}Tc was placed in the center of the FOV in the same plane as the detector. One image was obtained for each of the detectors. The sensitivity was calculated to

$$K_{^{99m}Tc} \approx 23 \ cps/MBq$$

A measurement of the sensitivity for ^{123}I was also performed with the same detector geometry, choice of collimator and couch position as the above measurements. The matrix size, scan speed and scan length were also the same as above. The main energy window were set to 20 % centered about the photopeak at 159 keV. The sensitivity for ^{123}I was determined to

$$K_{^{123}I} \approx 16 \ cps/MBq$$

4.3 Narrow beam attenuation coefficient

To obtain the narrow beam attenuation coefficient for the correction factors used in the Kojima background correction method, a number of values for μ_0, (for H_2O), were taken from the NIST website [12]. These values were plotted in a diagram with μ_0 as a function of photon energy. The function $y = 0,8067 \cdot x^{-0,3357}$ was conformed to the values and from this equation μ_0 for the energy 140 keV (for ^{99m}Tc) and 159 keV (for ^{123}I) was calculated.

Table 2: Narrow beam attenuation coefficients for photon energies between 60 and 300 keV.

Energy (keV)	μ_0
60	0.2059
80	0.1837
100	0.1707
140	0.1536
150	0.1505
159	0.1471
200	0.1370
300	0.1186

4.4 Effective attenuation coefficient

The effective attenuation coefficient for ^{57}Co was calculated for each organ by eq. 9 and transformed to the effective attenuation coefficient for ^{99m}Tc using eq. 10. The attenuation coefficients for each organ are presented in Table 3 below.

Table 3: Effective attenuation coefficients for the different organs in the MIRD phantom.

Phantom	$\mu_{eff_{Co}}$	$\mu_{eff_{Tc}}$	μ_{eff_I}
Liver	0.132	0.126	0.121
Kidneys	0.127	0.121	0.116
Heart	0.137	0.131	0.125
Intestine	0.129	0.124	0.118

4.5 Cylinder phantom measurements

The three spheres were filled with an amount of activity of 5.1 MBq, 3.1 MBq and 1.5 MBq of ^{99m}Tc respectively, (figure 9 shows the activity distribution in the phantom). In the cylinder phantom measurements four different combination of corrections were made: a) solely attenuation correction, b) attenuation- and Gates background correction, c) attenuation- and Kojima background correction, d) attenuation- and Bujis background correction, showing an underestimation in the activity quantification of 9 - 30 % (Table 4).

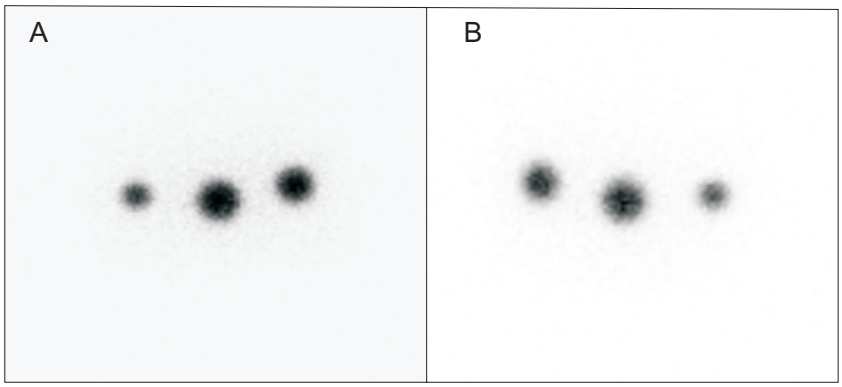

Figure 9: A: Anterior and B: posterior image from emission measurements of the cylindrical phantom containing three ^{99m}Tc-filled spheres of various size.

4.5.1 ^{99m}Tc measurements of the MIRD phantom

The amount of activity, (^{99m}Tc), that was added to the organ phantoms were: liver phantom 44.5 MBq, kidney phantoms 17.15 MBq, heart phantom 12.2 MBq and the small intestine phantom 7,8 MBq. Four liver-to-background concentration ratios were used, (infinity, 10:1, 5:1 and 2:1). An image of the

Table 4: Deviation of calculated activity from true activity in emission measurements on cylinder phantom.

Method	Sphere 1 (19 ml)	Sphere 2 (11 ml)	Sphere 3 (6 ml)
Attenuation	-29%	-10%	-10%
Att. + Gates	-30%	-12%	-13%
Att. + Kojima	-27%	-9%	-10%
Att. + Bujis	-27%	-9%	-10%

distribution of ^{99m}Tc in the various organs is shown in Figure 10 (organ-to-background concentration ratio 5:1).

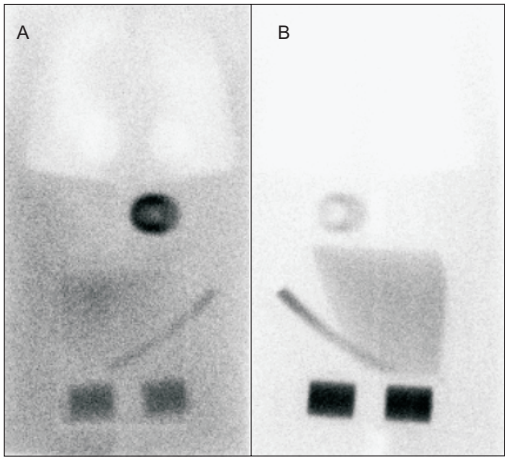

Figure 10: A: Anterior and B: posterior image from the emission measurements of the MIRD phantom containing ^{99m}Tc-filled liver, kidneys, heart and small intestine phantom. Liver-to-background concentration ratio 5:1.

In the diagrams showing the results of the measurements, each correction method is defined by a number which is given in figure 11.

Since the results from both the kidneys were virtually identical, only results from one of the kidneys are presented here.

When using only attenuation correction the deviation from the true activity value, (for the liver), ranged between an overestimation of 32 % and 125 % gradually increasing with decreasing liver-to-background concentration ratio. For the kidney phantoms the overestimation ranged between 15% for background concentration ratio of infinity and 76% for organ-to-background concentration ratio 2:1.

1. Attenuation correction, transmission measurements.
All of the following methods include attenuation correction.
2. TEW scatter correction.
3. DEW scatter correction.
4. LEW scatter correction.
5. TEW scatter correction and Gates background correction.
6. DEW scatter correction and Gates background correction
7. LEW scatter correction and Gates background correction
8. TEW scatter correction and Kojima background correction
9. DEW scatter correction and Kojima background correction
10. LEW scatter correction and Kojima background correction
11. TEW scatter correction and Bujis background correction
12. DEW scatter correction and Bujis background correction
13. LEW scatter correction and Bujis background correction.

Figure 11: Overview of methods used in this study. TEW is the Triple energy window method, DEW the double energy window method and LEW the lower energy window method. The numbers corresponds to numbers in diagrams showing the results of the measurements.

Table 5: Percentage deviation from true activity for the kidneys. The count rates are attenuation- and scatter corrected. No background correction was made.

Background conc ratio	Att. + TEW	Att. + DEW	Att. + LEW
Infinity	-9%	1%	13%
10:1	37%	35%	75%
5:1	89%	97%	121%
2:1	57%	70%	93%

When scatter corrections were added, the activity for the kidney phantoms ranged from 1% for attenuation correction combined with TEW and with no background activity, to 121% for organ-to-background concentration ratio of 5:1, attenuation and the LEW correction method (Table 5).

The activity for the liver phantom was underestimated for TEW and DEW with -13% and -3%, respectively (no background activity) and LEW method overestimated the activity with 12%. For decreasing organ-to-background concentration ratio the deviation from the true activity became higher for all three correction methods (Table 6).

For the heart phantom the overestimation was high for lower background concentration ratios and with the TEW method the deviation ranged between -18 and 132%, the DEW method -8 and 118% and with the LEW method from 1% to 178% overestimation (Table 7).

Table 6: Percentage deviation from true activity for the liver. The count rates are attenuation- and scatter corrected. No background correction was made.

Background conc ratio	Att. + TEW	Att. + DEW	Att. + LEW
Infinity	-13%	-3%	12%
10:1	28%	32%	75%
5:1	56%	63%	79%
2:1	150%	168%	141%

Table 7: Percentage deviation from true activity for the heart. The count rates are attenuation- and scatter corrected. No background correction was made.

Background conc ratio	Att. + TEW	Att. + DEW	Att. + LEW
Infinity	-18%	-8%	1%
10:1	11%	34%	85%
5:1	46%	36%	59%
2:1	132%	118%	178%

When the conventional background correction (Gates method) and the TEW scatter correction method were used (with no background activity) the activity was underestimated for all organs, (liver: -14%, kidneys: -10%, heart: -19%). An increase of the background concentration ratio, (2:1), resulted in an underestimation of -83% for the liver, -52% for the kidneys and -59% for the heart. The use of Gates method and DEW led to an underestimation of for example -10% for the kidneys and as above an increase in underestimation with decreasing background activity ratio (Figure 12).

When the Kojima background correction method was applied in conjunction with the three different scatter correction methods, the results improved to an underestimation within a range of -1% to -20% for all the organs.

Most accurate was the combination of the Gates method and the LEW method for the liver, were the activity varied from -1.7% (no background activity) to -16% for organ-to-background concentration ratio 10:1 and to 6% for organ-to-background concentration ratio 5:1 (Figure 14). Due to low count statistic the lowest organ-to-background concentration ratio did not give reliable results. The Bujis method gave similar results when applied to the values obtained from the 2:1 background measurement.

The Bujis method combined with the three scatter correction methods resulted in differences between true and calculated activity of 10 - 20 % for the TEW and the DEW method and zero background. The LEW method showed results of 1.4%, 1.6% and -0.6% for the liver, kidney and heart, respectively. For background concentration 10:1 the LEW greatly overesti-

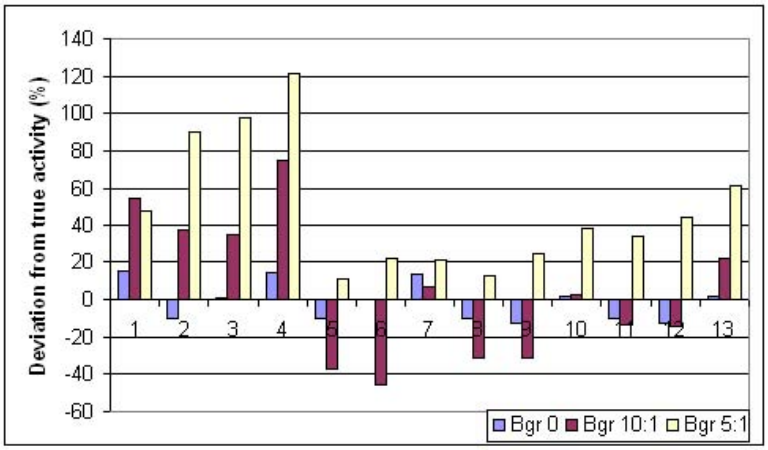

Figure 12: Deviation in % from true activity for kidney phantoms containing ^{99m}Tc, for liver-to-background concentration ratios of infinity, 10:1 and 5:1. The numbers on the x-axis are described in fig. 11.

mated the activity and the TEW and DEW gave similar results as for the zero background case (Figure 15).

Correction for overlapping organ was applied for the liver and small intestine. The activity estimation for the small intestine with only attenuation correction, (no background activity), was calculated to 32% from the true activity and with scatter correction according to TEW, DEW and LEW the deviation was -13%, -16% and -3% for each correction method. In combination with Gates background correction method the values for the scatter correction methods were -17%, -14% and -4% and scatter correction in combination with the Kojima method resulted in values of -17%, -21% and 0.4%. For the three scatter correction methods combined with Bujis correction method resulted in values of -17%, 21% and 0.3%.

4.5.2 ^{123}I measurements on the MIRD phantom

In the ^{123}I measurement 36.8 MBq was added to the liver phantom, 17.0 MBq each to the kidneys, 12.2 MBq to the heart and 8.3 MBq was added to the small intestine phantom. Image of the distribution of ^{123}I in the MIRD phantom is shown in Figure 16.

As for the ^{99m}Tc measurements, only applying attenuation correction greatly overestimated the activity in the phantom. The overestimation increased with decreasing background activity ratio and ranged between 133% and 204% for the liver (figure 17), 61% and 126% for the kidneys (figure 18)

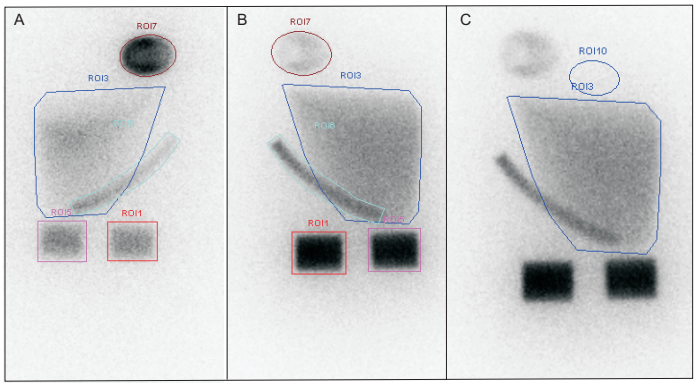

Figure 13: A: ROI:s in the anterior image. B: ROI:s in the posterior image. C: Smaller background ROI drawn in the image for use in the background correction for the liver.

and 82% and 142% for the heart (figure 19).

The scatter correction reduced the overestimation for the zero background case to 31% 43% and 50% for the liver (figure 17), 11% 15% and 6% for the kidneys (figure 18) and 23%, 26% and 19% for the heart (figure 19) for the TEW, DEW and LEW methods, respectively.

Using the Gates method in the background correction led to an underestimation of the activity for almost all of the methods except for the Gates background correction method in combination with the DEW method for the liver and heart, which instead gave an overestimation in the range of 3 - 13 %.

When using the Kojima method combined with the three different scatter corrections, the activity values for the liver were -26%, 6% and -1% for the TEW, DEW and LEW scatter correction method respectively (figure 17). For the kidneys, the corresponding values were -30%, -20% and -29% for background concentration ratio of infinity. When the background were increased to 10:1, the underestimation became smaller, for example for the kidneys with Kojima and the TEW method, (-3%)(figure 18). The Bujis method gave an overestimation for the liver and an underestimation for the kidneys and the heart.

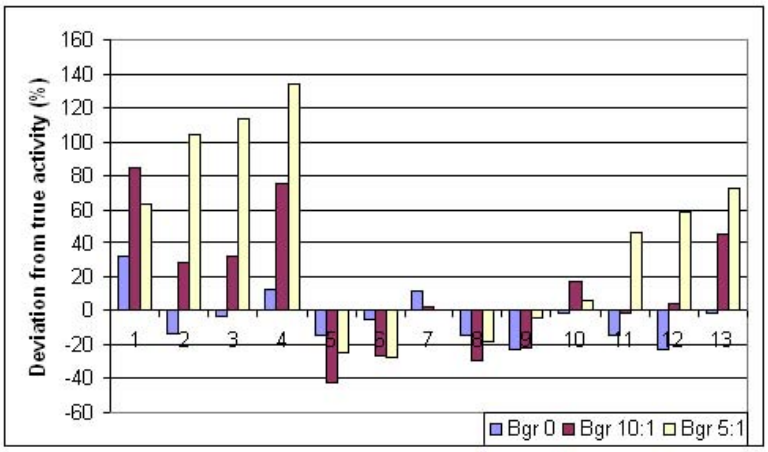

Figure 14: Deviation in % from true activity for liver phantom containing ^{99m}Tc, for liver-to-background concentration ratios of infinity, 10:1 and 5:1. The numbers on the x-axis are described in fig. 11.

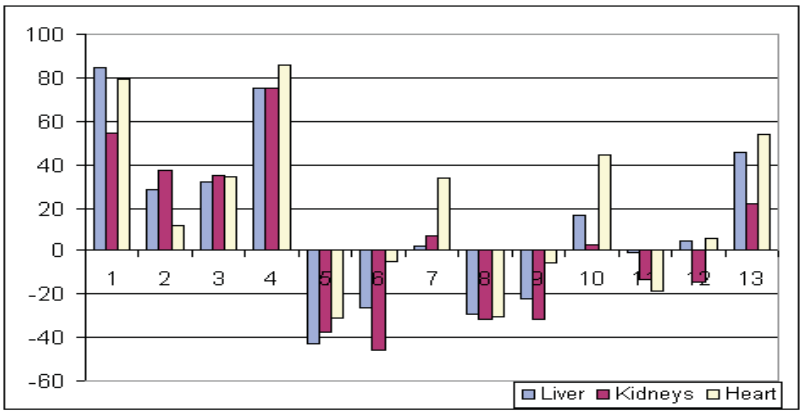

Figure 15: Deviation in % from true activity for the liver, kidney and heart phantoms containing ^{99m}Tc, for liver-to-background concentration ratio of 10:1. The numbers on the x-axis are described in fig. 11.

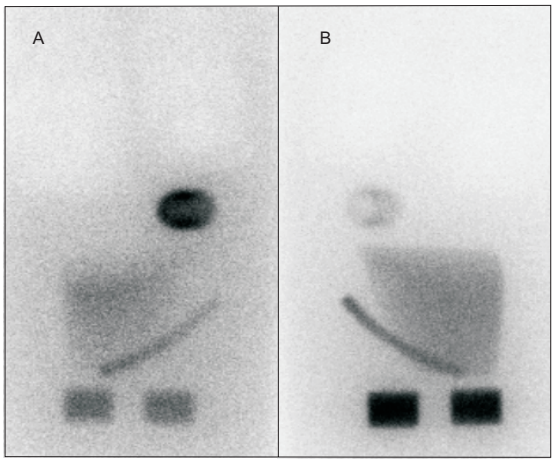

Figure 16: Image of the distribution of ^{123}I in the MIRD phantom. A: Anterior and B: posterior image. Liver-to-background concentration ratio 10:1.

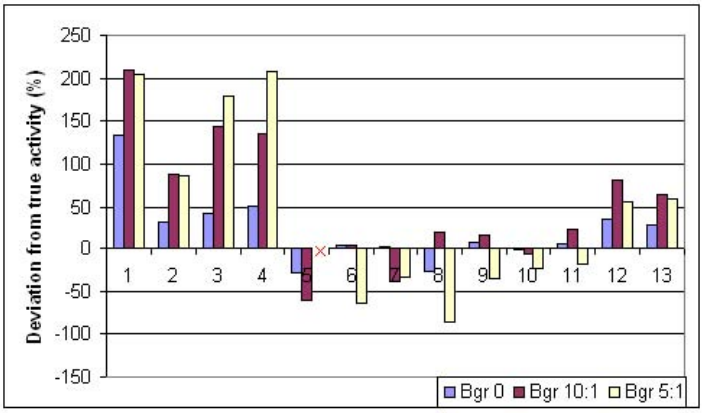

Figure 17: Deviation in % from the true activity values for ^{123}I for the liver with a liver-to-background concentration ratio of infinity, 10:1 and 5:1. The numbers on the x-axis are described in fig. 11.

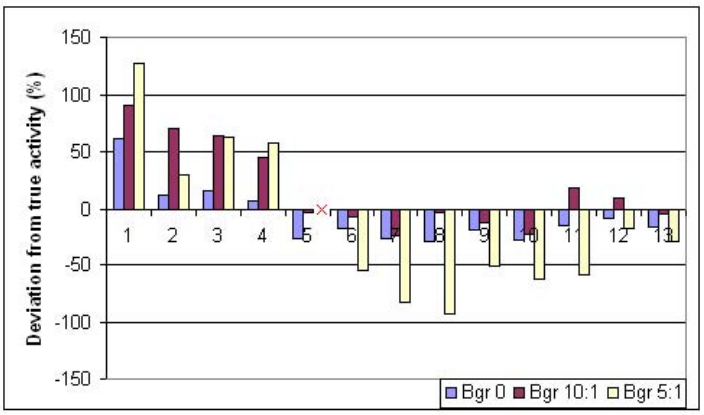

Figure 18: Deviation in % from the true activity values for ^{123}I for the kidneys with a liver-to-background concentration ratio of infinity, 10:1 and 5:1. The numbers on the x-axis are described in fig. 11.

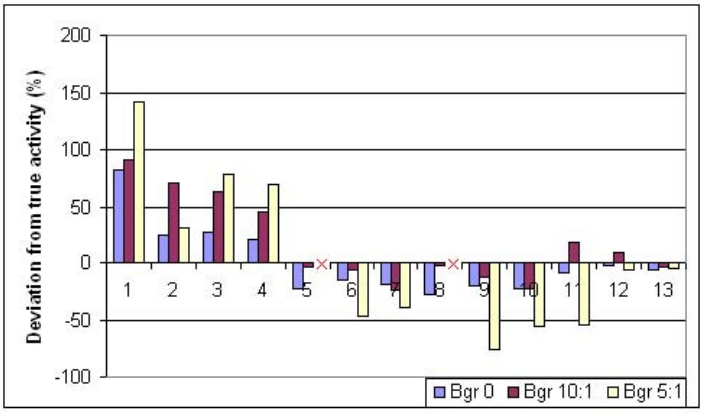

Figure 19: Deviation in % from the true activity values for the heart containing ^{123}I, with liver-to-background concentration ratios of infinity, 10:1 and 5:1. The numbers on the x-axis are described in fig. 11.

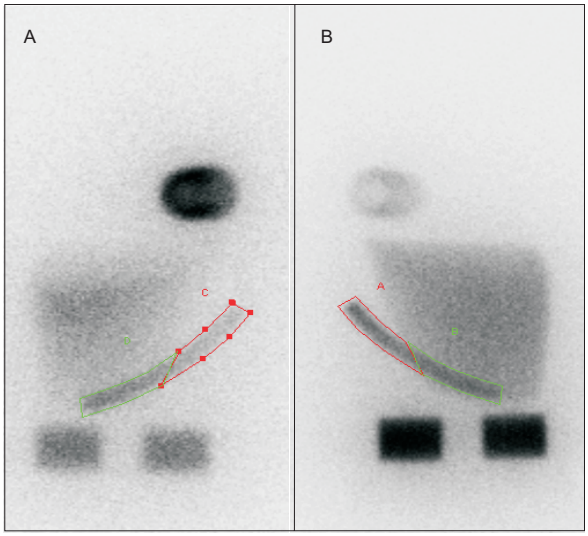

Figure 20: ROI:s drawn in the A: anterior and B: posterior image for the correction of overlapping structure.

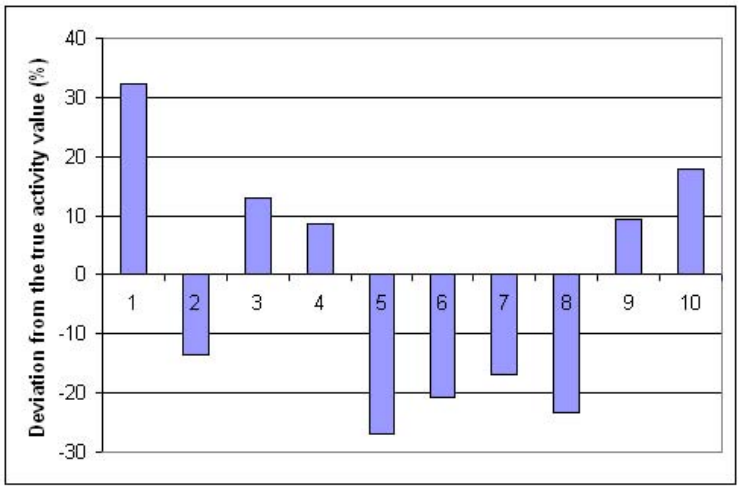

Figure 21: Deviation in % for calculated activity for the small intestine containing ^{123}I, with a liver-to-background concentration ratio of infinity. The numbers on the x-axis are described in fig. 11.

Correction for overlapping organ was carried out for the liver and small intestine (figure 21). ROI:s were drawn in the images as shown in Figure 20. The activity estimation for the small intestine with only attenuation correction, (no background activity), was calculated to 32% from the true activity value and with scatter correction according to TEW, DEW and LEW the deviation was -14%, 13% and 9% for each correction method. In combination with Gates background correction method the values for the scatter correction methods were -27%, -21% and -17% and scatter correction in combination with the Bujis method resulted in values of -23%, 9% and 18%.

5 Discussion

To perform an accurate quantification of the organ activity content from planar gamma camera images, several corrections has to be made. Two important factors that influences the results of the quantification is the attenuation and the scattering of photons in the organs and surrounding tissue. In this study, one method of attenuation correction and three different methods of scatter correction were used, (TEW, DEW and LEW). These methods have been studied among others by Ljungberg *et al.* [4], which showed that the use of the DEW method generated a complication, which was the choice of k-value used. The generally accepted k-value of 0.5 was used in the study of Ljungberg, as in this present study. The TEW method, which included two scatter windows of equal width intended to be more sensitive to noise, and thus a less accurate method than the LEW method in which the upper scatter window was set to zero and the lower window was used as in the TEW method. The results of that study showed that the TEW method greatly overestimated the scatter in the phantom and the LEW method underestimated the scatter but was more accurate.

In this study, the TEW method overestimated the scatter and thus underestimated the activity in the liver phantom. The LEW method gave an overestimation of activity to a lesser extent than for the TEW method. When considering large organs as the liver, and using ^{99m}Tc, the DEW method seemed to be the most accurate method for scatter correction, (-3%). Since this larger organ produces more scatter, one could expect the DEW method to be the most accurate as it subtracts the largest amount of scatter from the main window. But for the smaller organs, the kidneys and especially the heart, the use of the LEW scatter correction method showed great accuracy, (1.5% for ^{99m}Tc and zero background). The LEW method has, as mentioned before, shown more accurate results than the TEW method for measurements with ^{99m}Tc.

In a study by Delpon *et al.* [2] a comparison between the TEW and the DEW method showed that for small patients, the DEW method was more accurate than the TEW method and for average sized patients, the TEW was slightly more accurate than the DEW method.

The ^{123}I-measurements did not give the same results as the ones achieved for the ^{99m}Tc-measurements. The reason could be the difference in characteristics between the two radionuclides. In the ^{123}I decay, several high energy photons are emitted, which causes a larger amount of scatter in the higher energy window. This could explain that the deviation from the true activity values for the liver were highest when using the LEW method, (50%), because when setting the higher energy window to zero, a large amount of scattered photons might not be taken into account. The deviation from the true activity values was lower for the TEW method, (43%), and the most accurate method in this case were the DEW method, (31%).

The activity was overestimated to a lesser extent in the heart with the LEW method as the most accurate method with an overestimation of 19%. The most accurate activity value was obtained for the kidneys and the LEW method, which gave an overestimation of 6%. With respect to quantification with the three scatter correction methods, the LEW is the most accurate method when quantifying activity in small organs. The least accurate method for smaller organs was the DEW method. A reason that the LEW method showed more accurate results in this case than the DEW method (with ^{123}I), could be that both the correction methods lack the higher energy window, and the DEW method subtracts a larger amount of scatter than the LEW method. In organs as small as the kidneys, the amount of scatter is overestimated by the DEW method.

Correction for background activity was done by three different correction methods: the conventional background correction method, (Gates), the Kojima correction method and the Bujis correction method. The Gates, Kojima and Bujis correction methods were studied and compared by Bujis *et al.* [5], but with no scatter correction as in this study. The results of the Bujis study showed that the Kojima method was the most accurate method for quantification of activity in the kidneys, the Bujis method showed only slightly less accurate results and the conventional background subtraction greatly underestimated the activity in the kidneys.

For zero background activity, in this study the Bujis method was the most accurate for all of the organs when using ^{99m}Tc. When studying the Bujis and each of the three scatter correction methods, it was found that the combination of Bujis and LEW gave the most accurate results: -1.3% for the liver, 1.6% for the kidneys and -0.6% for the heart.

When the background activity was increased to a ratio of 10:1, the Kojima and LEW methods made the best set of correction methods regarding the kidneys with an overestimation of activity of only 2.6% for ^{99m}Tc. Regarding the heart, the three background correction methods gave similar results when used with the DEW method, but the Gates method were more accurate, (-5%). The TEW method were the most accurate for the liver and combined with the Bujis method it resulted in an underestimation of only 1%.

For higher background activity, (^{99m}Tc), the Bujis method showed more accurate results for the heart (-5.3%) especially together with the LEW scatter correction method, but for the liver, the LEW method combined with the Kojima method gave the most accurate results (-18%). For the kidneys the Gates method combined with the DEW for scatter correction gave an activity value that deviated from the true activity value with -10%.

At background concentration ratio of 10:1, (^{123}I), the Kojima method is more accurate than the other background correction methods. In combination with the LEW method, a difference of -2.6% was found.

6 Conclusions

In this study, the influence of three different scatter correction methods and three background correction methods on the activity quantification of three types of organ phantoms has been studied.

To find the most suitable set of correction methods is very complicated and demands several studies to get statistical significance in the results. But an indication of which set is the best one can be seen in this study.

When using ^{99m}Tc, the combined use of Bujis background- and LEW scatter correction methods yielded very accurate results, for both low and high background concentration ratios. It also showed that for large organs, the TEW method gave very accurate results as did the DEW scatter correction method for smaller organs.

When instead using ^{123}I, the most accurate results of attenuation and scatter correction was obtained for large organs when applying the TEW method. For smaller organs, the LEW method was the most accurate method for scatter correction. The combined use of TEW scatter correction method and Bujis background correction method yielded slightly more accurate results than the combination of other correction methods.

As seen in this study, there is not only one set of correction methods which gives the most accurate results in all cases, there is different sets that is suitable for different situations. When considering the different radionuclides

used in this study, corrections made after the use of ^{99m}Tc, showed greater stability in the corrected activity values, and if the combination of methods is easy to implement, the choice can be the Bujis and the LEW method. But for ^{123}I, the situation is more complicated, and the results were varying. One could note an improvement with the TEW method in conjunction with the Bujis method. However, in a clinical situation, the most easily implemented method is most likely to be chosen, since the differences of the results between the different set of correction methods are small.

7 Acknowledgements

I would like to thank some people from whom I have received help during this work.

Sigrid Leide-Svegborn for excellent supervising.

Kristina Norrgren for sharing knowledge and time with me.

Kai Nilsson for helping me with radionuclides.

Sven Brink for fixing my kidney phantom.

The staff at the clinical physics department at UMAS for arranging time for me at the gamma cameras.

Magnus for being my biggest supporter.

References

[1] Fleming JS. *A technique for the absolute measurement of activity using a gamma gamera and computer.* Phys Med Biol 1979;24:176-180.

[2] Delpon G, Ferrer L, Lenta C, Lisbona A, Buvat I, Bardiés M. *Comparison of four scatter correction methods for patient whole-body imaging during therapeutic trials with Iodine-131.* Cancer. 2002 Feb 15; 94(4 Suppl):1224-30.

[3] Ronald J. Jaszcsak, Kim L Greer, Carey E. Floyd, Jr., C. Craig Harris and R. Edwaqrd Coleman *Improved SPECT Quantification Using Compensation for Scattered Photons.* J Nucl Med 1984; 25:893-900.

[4] Michael Ljungberg, Michael A. King, George J. Hademenos, Sven-Erik Strandh. *Comparison of four scatter correction methods using Monte Carlo simulated source distributions.* J Nucl Med 1994; 35:143-151.

[5] Wilhelmina C.A.M. Bujis, Jeffry A. Siegel, Otto C. Boerman, Frans H.M. Corstens. *Absolute organ activity estimated by five different methods of background correction.* J Nucl Med 1998; 39:2167-72.

[6] Leide-Svegborn S, Areberg J, Norrgren K, Mattsson S.*Accuracy of the quantification of organ content of radionuclides from planar gamma camera images.* Report MA RADFYS 99:01. Department of radiation physics, Malmö, Lund University.

[7] Kristina Norrgren, Sigrid Leide Svegborn, Johan Areberg, Sören Mattsson. *Accuracy of the quantification of organ activity from planar gamma camera images.* Cancer Biotherapy & Radiopharmaceuticals 2003; 18:125-131.

[8] Miles N. Wernick, John N. Aarsvold. *Emission tomography: The fundamentals of PET and SPECT.* Copyright 2004, Elsevier Inc. ISBN: 0-12-744482-3.

[9] Buvat I, Rodriguez-Villafuente M, Todd-Pokropek A, Benali H, Di Paola R. *Comparative Assessment of Nine Scatter Correction Methods Based on Spectral Analysis Using Monte Carlo Simulations.* J Nucl Med. 1995 Aug Vol 36(8), 1476-88.

[10] Gates GF. *Split renal function testing using Tc-99m DTPA: a rapid technique for determining differential glomerular filtration.* Clin Nucl Med 1983; 8:400-407.

[11] Takaki Y, Kojima A, Tsuji A, Nakashima R, Tomiguchi S, Takahashi M. *Quantification of Renal Uptake of Technetium-99m-DTPA Using Planar Scintigraphy: A technique That Considers Organ Volume.* J Nucl Med 1993;34:1184-1189.

[12] Website. *National institute of standards and technology*, NIST.

[13] Lena Jönsson, Michael Ljungberg, Sven-Erik Strandh. *Evaluation of accuracy in activity calculations for the conjugate view method from Monte Carlo simulated scintillation camera images using experimental data in an anthropomorphic phantom.* J Nucl Med 2005; 46:1679-1686.